Runx2 Disruption Promotes Immortalization and Confers Resistance to Oncogene-Induced Senescence in Primary Murine Fibroblasts

Anna Kilbey,[1] Karen Blyth,[1] Sandy Wotton,[1] Anne Terry,[1] Alma Jenkins,[1] Margaret Bell,[1] Linda Hanlon,[2] Ewan R. Cameron,[1] and James C. Neil[1]

[1]Molecular Oncology Laboratory, Institute of Comparative Medicine, Faculty of Veterinary Medicine, University of Glasgow, Glasgow, United Kingdom and [2]J. Kissil Laboratory, The Wistar Institute, Philadelphia, Pennsylvania

Abstract

The *Runx* genes play paradoxical roles in cancer where they can function either as dominant oncogenes or tumor suppressors according to context. We now show that the ability to induce premature senescence in primary murine embryonic fibroblasts (MEF) is a common feature of all three *Runx* genes. However, ectopic Runx–induced senescence contrasts with Ras oncogene–induced senescence, as it occurs directly and lacks the hallmarks of proliferative stress. Moreover, a fundamental role for Runx function in the senescence program is indicated by the effects of *Runx2* disruption, which renders MEFs prone to spontaneous immortalization and confers an early growth advantage that is resistant to stress-induced growth arrest. *Runx2*$^{-/-}$ cells are refractory to H-Ras^{V12}–induced premature senescence, despite the activation of a cascade of growth inhibitors and senescence markers, and are permissive for oncogenic transformation. The aberrant behavior of *Runx2*$^{-/-}$ cells is associated with signaling defects and elevated expression of S-G$_2$-M cyclins and their associated cyclin dependent kinase activities that may override the effects of growth inhibitory signals. Coupling of stress responses to the cell cycle represents a novel facet of Runx tumor suppressor function and provides a rationale for the lineage-specific effects of loss of Runx function in cancer. [Cancer Res 2007;67(23):11263–71]

Introduction

The three members of the *Runx* family of mammalian transcription factors are related to *Runt*, the Drosophila pair rule gene (1), sharing a highly conserved DNA-binding domain and a common DNA-binding cofactor. Their products regulate multiple cell fate decisions and have been implicated in a wide range of cancers where there is unequivocal evidence that members of this family can act as oncogenes or as tumor suppressors according to context (2).

The identification of somatic and germ-line loss-of-function mutations associated with acute myeloid leukemia (AML) strongly supports the view that *RUNX1* operates as a tumor suppressor gene in this lineage. Further evidence that the *RUNX* genes can inhibit tumor development comes from a number of reports suggesting that methylation and down-regulation of *RUNX3* is etiologically associated with the development and progression of a spectrum of epithelial cancers (ref. 2 and references therein). However, it is clear that the tumor suppressor role of the *RUNX* gene family is expressed in a lineage-restricted manner. Functional redundancy and partially overlapping expression patterns of the three family members have been proposed to account for these observations. Functional similarity between the *Runx* genes is also suggested by the finding that all three genes act as a single complementation group by retroviral activation in experimental models of hematologic malignancy (3–5).

The mechanisms underlying these contrasting manifestations in cancer are not fully understood, although it seems that ectopic Runx expression can inhibit apoptosis, particularly in transgenic mice overexpressing the *Myc* gene. Moreover, the growth suppressive features of Runx2 are evident in this T-cell transgenic model, as prelymphomatous mice display a proliferative defect in immature thymocytes, which is overcome by ectopic Myc expression (6). Loss of *Runx1* seems to result in increased proliferation and failure of hematopoietic precursor cells to differentiate (7), suggesting that homeostatic control of hematopoiesis is a central function of this gene, whereas *RUNX3* down-regulation and hypermethylation in epithelial cells has been linked to loss of growth inhibitory responses to transforming growth factor-β (TGF-β; refs. 8, 9). Together, these observations are consistent with growth inhibitory Runx functions that are selectively lost in cancers or overcome by complementing oncogenic mutations affecting collaborating genes, such as *Myc* or *p53*, which serve to reveal the oncogenic side of their dual nature (10, 11). However, it is not known whether these various inhibitory phenomena represent shared functions across family members and in different lineages, or whether they can fully account for the tumor suppressor activities of this gene family.

A striking demonstration of *RUNX*-induced negative growth regulation is the senescence-like phenotype observed after ectopic expression of *RUNX1* in primary murine embryonic fibroblasts (MEF; refs. 11, 12). Premature senescence or growth stasis shares many of the characteristics of replicative senescence but is independent of telomere shortening and occurs in response to activation of stress pathways that detect or heighten cellular responses to DNA damage (13). Thus, the aberrant expression of oncogenes, such as activated Ras, can result in a transient round of cell proliferation followed by permanent withdrawal from the cell cycle and other phenotypic features indicative of cellular senescence. Moreover, it is now clear that this is not merely a feature of *in vitro* conditions and that this phenomenon limits tumor development *in vivo* (14, 15). Although species and cell type differences exist, many of the essential components of the Ras-induced senescence pathway have been identified and there is considerable overlap between these components and genes with

Requests for reprints: Anna Kilbey, Institute of Comparative Medicine, Glasgow University Veterinary School, Bearsden Road, Glasgow G61 1QH, United Kingdom. Phone: 44-141-330-3444; Fax: 44-141-330-2271; E-mail: A.Kilbey@vet.gla.ac.uk or James C. Neil, Institute of Comparative Medicine, Glasgow University Veterinary School, Bearsden Road, Glasgow G61 1QH, United Kingdom. Phone: 44-141-330-2365; E-mail: j.c.neil@vet.gla.ac.uk.

doi:10.1158/0008-5472.CAN-07-3016

established tumor suppressor function. In accord with this hypothesis activation of the major tumor suppressor pathways mediated by p53 and/or pRb family members is a hallmark of premature senescence (16).

We now report that induction of premature senescence in MEFs is a common feature of all three *Runx* genes. However, this process differs markedly from Ras-induced senescence as it occurs without an initial aberrant proliferative phase. Moreover, MEFs lacking *Runx2* display an early growth advantage that is resistant to *in vitro* culture stress and are susceptible to H-Ras^{V12}–induced cellular transformation. Our results suggest that *Runx* genes play a central role in regulating the cell cycle in response to stress signals, including ectopic oncogene expression, offering new insights into the mechanisms of Runx tumor suppression.

Materials and Methods

Cells, constructs, and retroviral transductions. Littermate wild-type and *Runx2*$^{-/-}$ MEFs were prepared from E14.5 embryos derived from mating *Runx2*$^{+/-}$ mice (17). The virus packaging line Phoenix (ecotropic) was obtained from G. Nolan (Stanford University, Palo Alto, CA). All cultures were maintained in DMEM (Invitrogen) with 10% heat-inactivated FCS, glutamine (2 mmol/L), and penicillin/streptomycin (200 units/mL; 100 μg/mL). The retroviral vectors were all based on the pBabe plasmid (18), carrying the puromycin-selectable marker. pBabe-PURO *Runx2*, kindly provided by M. Stewart (Glasgow University, Glasgow, United Kingdom), comprises a 2.3-kb cDNA fragment encoding the *Cbfa1*-G$_1$ isoform (3) subcloned into the polylinker region of pBabe-PURO. pBabe-PURO *Ras* was kindly provided by S. Lowe (Cold Spring Harbor Laboratory, New York, NY; ref. 16). Retroviral transductions were performed as previously described (11).

Growth curves, senescence staining, and 3T3 passage culture. Early passage (p3–p4) MEFs were plated at 2.5×10^4 cells per well in 12-well plates in growth medium or in selection medium containing 2 μg/mL puromycin. Live cell counts were carried out in triplicate using trypan blue as a vital stain. Triplicate wells were pooled from each time point for analysis of protein expression. Medium changes were carried out every 3 to 4 days. For UVC irradiation, early passage MEFs were plated overnight at 5.0×10^5/60-mm dish. The medium was then removed, and the cells were irradiated using an XL-1500 UV cross-linker (Spectrolinker). The cultures were incubated in fresh medium, and live/dead cell counts were performed after 24 h by trypan blue exclusion. Graphs were plotted using Sigma plot, and significance values were determined by Student's *t* test. Error bars relate to SDs. Senescence staining was assayed on a parallel plate after 7 to 10 days using a solution of X-gal (Invitrogen) at pH 6.0 to detect senescence-associated β-galactosidase (SA-β-gal) activity as described previously (16). 3T3 passage culture was essentially performed according to the protocol of Todaro and Green (19).

Cell cycle analysis. MEFs plated at 3×10^5 cells/10-cm dish were sampled for flow cytometry in parallel with growth curves. The protocol for cell cycle analysis has been described previously (20). For simultaneous labeling with bromodeoxyuridine (BrdUrd), cells were incubated at 37°C with 10 μmol/L BrdUrd (Sigma) and then rinsed thrice in warmed PBS. After harvesting, cells were washed in 2 mL cold PBS, resuspended in 0.2 mL cold PBS, and fixed for at least 30 min in 2 mL of 70% ethanol at 4°C. Cells were denatured in 4 mol/L HCl for 20 min, rinsed twice in cold PBS, incubated for 10 min in PBS/0.5% bovine serum albumin/0.1% Tween 20, and labeled with FITC-conjugated anti-BrdUrd antibody (Roche). Samples were washed twice in PBS and resuspended in PBS containing 10 μg/mL propidium iodide. Analysis was carried out on a Beckman Coulter Epics XL using EXPO32 software.

Western blotting and antibodies. Preparation of whole cell protein extracts was performed as described previously (11). Samples equivalent to 30 μg total protein (Bio-Rad protein assay) were resolved on 8%, 10%, or 17% SDS-polyacrylamide gels and transferred to enhanced chemiluminescence (ECL; Amersham) nitrocellulose membranes. The antibodies used were α-p16^{INK4a}, α-p21^{WAF1}, α-actin (sc-1207, sc-471, and sc-1616, Santa Cruz Biotechnology), α-p19^{ARF} (ab80, Abcam), α-p53, α–phospho-p38 mitogen-activated protein kinase (MAPK), α-p38 MAPK (IC12, 9211, and 9212, Cell Signaling Technology), α–c-H-*ras* (Oncogene Ab-1), and α-RUNX2 (D130-3, Stratech). Western blots were developed using ECL according to the manufacturer's protocol. Positive controls were as follows: p16^{INK4a} and p19^{ARF} (SV3T3 cell extract), p21^{WAF1} and p53 (UVC-treated wild-type MEF extract) and p38 MAPK (Jurkat cell extract). Negative controls were as follows: p16^{INK4a} and p19^{ARF} (NIH3T3 cell extract), p21^{WAF1} (RAT 1 fibroblast extract) and p53 (p53 null MEF extract).

***In vivo* transplantation studies.** *Runx2*-null and wild-type MEFs were transduced with either the constitutive H-Ras^{V12} or PURO-vector control and expanded in culture for 7 days. Cells (10^6) in 0.2 mL PBS were injected s.c. into the left flank of 5 to 6 MFI *nu/nu* mice (Harlan) for each cell group. Animals were housed in sterile filter-top cages, monitored thrice weekly, and humanely sacrificed when tumor masses reached a predetermined size or became ulcerated. All animal work was undertaken in line with the United Kingdom Animals Act of 1986 (Scientific Procedures).

Colony assays. For soft agar colony assays, cells were diluted into 0.3% agar (Noble Difco) in DMEM containing 20% FCS and seeded in triplicate onto solidified 0.6% agar containing culture medium at 10^3, 10^4, or 10^5 cells/6-cm plate (Bibby Sterilin). The colonies were fed every 3 to 4 days and evaluated after 5 weeks.

RNA extraction and cDNA preparation. *Runx2*$^{-/-}$ and wild-type MEFs were transduced with either constitutive H-Ras^{V12} or the PURO-vector control and plated on six-well plates at 7.5×10^4 cells per well. The cells were harvested from triplicate wells at days 3, 7, 10, and 13 into 1-mL RNA-Bee (AMS Biotechnology), and RNA was prepared according to the manufacturer's protocol. RNA pellets were dissolved in diethyl pyrocarbonate (DEPC)-treated water (Ambion), and the concentration was determined using an Agilent Bioanalyzer. cDNA was prepared from 1-μg aliquots of RNA using a Quantitect Reverse Transcription kit (Qiagen) and diluted 1 in 20 in DEPC-treated water to give a working stock.

Quantitative real-time PCR. Five-microliter aliquots of cDNA were amplified in triplicate on an ABI 7500 real-time PCR system using Power SYBR Green PCR master Mix (Applera UK) and primers for murine cyclin A2, cyclin B1, cyclin E1 (Qiagen Quantitect Primer Assays QT00102151, QT00152040, and QT00103495), or endogenous control hprt (106F 5′-AGCGTCGTGATTAGCGATGAT-3′ and 253R 5′-CCTTCATGACATCTCGAG-CAAG-3′). Relative quantification was carried out and calibrated to day 0 wild-type sample.

***In vitro* kinase assays.** Immunoprecipitation kinase assays for cyclin A–, cyclin B1–, and cyclin E–associated kinase activities with histone H1 as a substrate were performed as described previously (21). Essentially *Runx2*$^{-/-}$ and wild-type MEFs were plated at 1.5×10^6 cells/150-mm dish and grown to 80% to 90% confluence for 4 to 5 days. The contents of one dish were extracted into 0.5-mL lysis buffer, and the protein concentrations were determined as for Western extraction. Five hundred micrograms of total cellular extract were analyzed per reaction. Monoclonal antibodies against cyclin A (MAB3682, Chemicon) and cyclin B1 (sc-245, Santa Cruz Biotechnology) were used to immunoprecipitate cyclin A– and cyclin B1– associated kinase complexes directly. For cyclin E–associated kinase activity, cell lysates were sequentially immunoprecipitated with α-cyclin A and α-CDK2 (sc-163; Santa Cruz Biotechnology). Kinase reactions were transferred to nitrocellulose membranes for autoradiography.

Results

Induction of premature senescence in primary mouse fibroblasts is a common feature of the Runx family but is distinct from H-Ras^{V12}–induced senescence. We previously showed that *RUNX1* mediates senescence-like growth arrest in

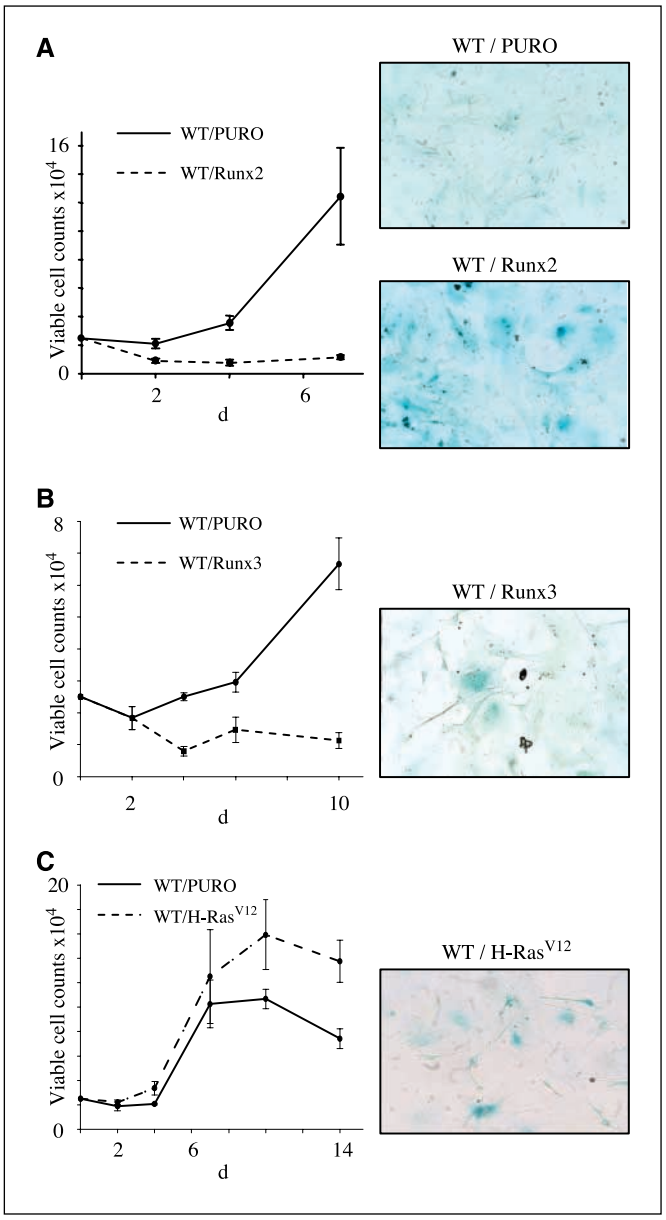

Figure 1. Runx2 and Runx3 induce a senescence-like growth arrest in wild-type (*WT*) MEFs that is distinct from H-Ras^{V12}. *A,* cells were transduced with a vector containing *Runx2* or a control vector containing the *PURO*-selectable gene. Growth curves showing viable cell numbers of Runx2 (*dashed line*) and vector control (*solid line*) cells are shown. Similar results were obtained in two independent experiments. SA-β-gal staining of matched day 8 cultures are displayed. Photographs are at the same magnification. *B,* parallel growth curves and SA-β-gal staining in wild-type MEFs transduced with a vector containing *Runx3* (*dashed line*) and (*C*) mutant *H-Ras^{V12}* (*dashed line*).

primary MEFs (11). To determine whether this response is a general property of the *Runx* family, we tested the effect of introducing ectopic *Runx2* into wild-type cells by retroviral transduction. Western blot analysis revealed high intracellular levels of ectopic Runx2 and a corresponding dramatic reduction in cell numbers over a 7-day culture period (Fig. 1*A*). In contrast, cells carrying the control vector (PURO control) showed at least a 10-fold increase in cell number over the same period. Moreover, cells expressing ectopic Runx2 displayed a senescent-like phenotype characterized by an enlarged flattened appearance and SA-β-gal staining. These results clearly show that ectopic Runx2 can induce a profound growth arrest in cultured cells and implicate Runx2 as a direct mediator of this response. Parallel experiments with Runx3 gave essentially identical results (Fig. 1*B*). However, this phenomenon differed from premature senescence induced by H-Ras^{V12} in primary MEFs, which produced an early proliferative response followed by a sustained growth arrest with retention of fibroblastic and spindle shapes in a proportion of the culture (Fig. 1*C*). Although H-Ras^{V12}–induced senescence seems to be activated in response to aberrant cellular proliferation (ref. 22 and references therein), Runx-induced senescence is a more direct process reflecting negative growth regulation.

***Runx2*$^{-/-}$ fibroblasts are prone to spontaneous immortalization and display an early growth advantage *in vitro*.** Analysis of *Runx* gene family expression in primary MEFs by Western blot and gene expression microarray revealed that *Runx2* is the most abundantly expressed family member, and this observation led us to consider the possibility that this gene has a nonredundant role in their growth regulation. Under typical culture conditions, primary MEFs exit the cell cycle in increasing numbers during passage, resulting in eventual growth stasis (19). The use of a 3T3 passage protocol can occasionally permit the accumulation of secondary events that serve to immortalize primary cells *in vitro*. Using this approach, we observed cessation of growth in six out of six cultures of wild-type MEFs (Fig. 2*A*). In contrast, five of six lines derived from *Runx2*$^{-/-}$ embryos exhibited an enhanced growth rate around passages 8 to 10, indicating the emergence of clones with an increased proportion of proliferating cells (Fig. 2*A*). Further study revealed that these cells were immortalized and, unlike their wild-type counterparts, could grow beyond passage 25 with little or no sign of reduced proliferation. However, these cells remained nontumorigenic in immunocompromised mice.

To further investigate the nature of their growth deregulation, we examined the properties of early passage *Runx2*$^{-/-}$ MEFs. As shown in Fig. 2*B*, *Runx2*$^{-/-}$ cells expanded significantly faster than litter-matched controls over 7 days in culture. Flow cytometry analysis of BrdUrd accumulation indicated that the increase in total cell count was due, at least in part, to increased cell division in the *Runx2*$^{-/-}$ cultures (Fig. 2*C*). However, we noted that the overall rates of proliferation of early MEF cultures were very low compared with established 3T3 fibroblasts (Fig. 2*C*), with only 10% of control cells taking up BrdUrd over a 3-h period.

Primary rodent fibroblasts display a progressive loss in proliferative capacity in culture that has been attributed to culture stress and may account for the low proliferative rates of primary MEFs observed in this study (23, 24). To determine whether the growth advantage of *Runx2*$^{-/-}$ fibroblasts was a consequence of reduced sensitivity to "culture shock," cells of both genetic backgrounds were plated at passages 3, 5, and 7, and their growth was compared over 7 days in culture. As shown in Fig. 3*A*, *Runx2*$^{-/-}$ fibroblasts retain a greater proliferative capacity than their wild-type counterparts with successive passages but have not lost their sensitivity to replication-induced growth inhibition. In contrast, differential susceptibility was seen in the response to low-dose UVC, where *Runx2*$^{-/-}$ cells showed increased viability relative to their wild-type counterparts (Fig. 3*B*). In view of evidence that the *Runx* genes play important roles in negative growth regulation by TGF-β in a range of cell types (9, 25, 26), we also tested the effects of *Runx2* disruption on this response. Surprisingly, we saw no

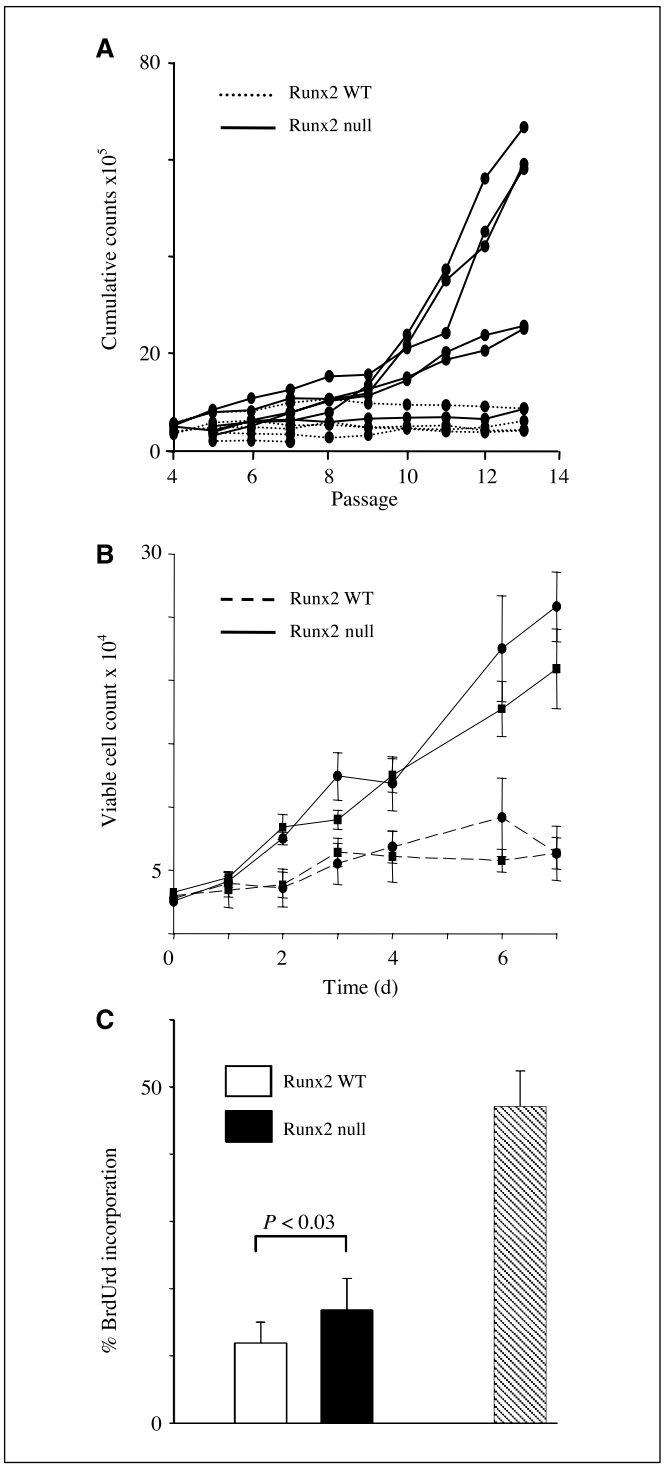

Figure 2. *Runx2*$^{-/-}$ fibroblasts are prone to secondary events that lead to immortalization. *A,* 3T3 passage culture was performed on five wild-type and six *Runx2*$^{-/-}$ lines. Cells were plated at 3.0×10^5/T25 flask and passaged every 3rd day, reseeding 3.0×10^5 cells into a fresh flask. The increase in total viable cell numbers was calculated at every passage and added to a cumulative count over time. Secondary events that predispose to immortalization occurred between passage 8 and 10. *B, Runx2*$^{-/-}$ fibroblasts display an early growth advantage *in vitro*. Growth curve of two *Runx2*$^{-/-}$ lines compared with two wild-type lines seeded at passage 4. The experiment was repeated on six littermate-matched *Runx2*$^{-/-}$ and wild-type lines with essentially identical results. *C,* the percentage of BrdUrd incorporation in three *Runx2*$^{-/-}$ and three wild-type lines seeded at passage 5 and labeled for 3 h. A comparison is shown for NIH3T3 cells labeled for 1 h (*hatched column*).

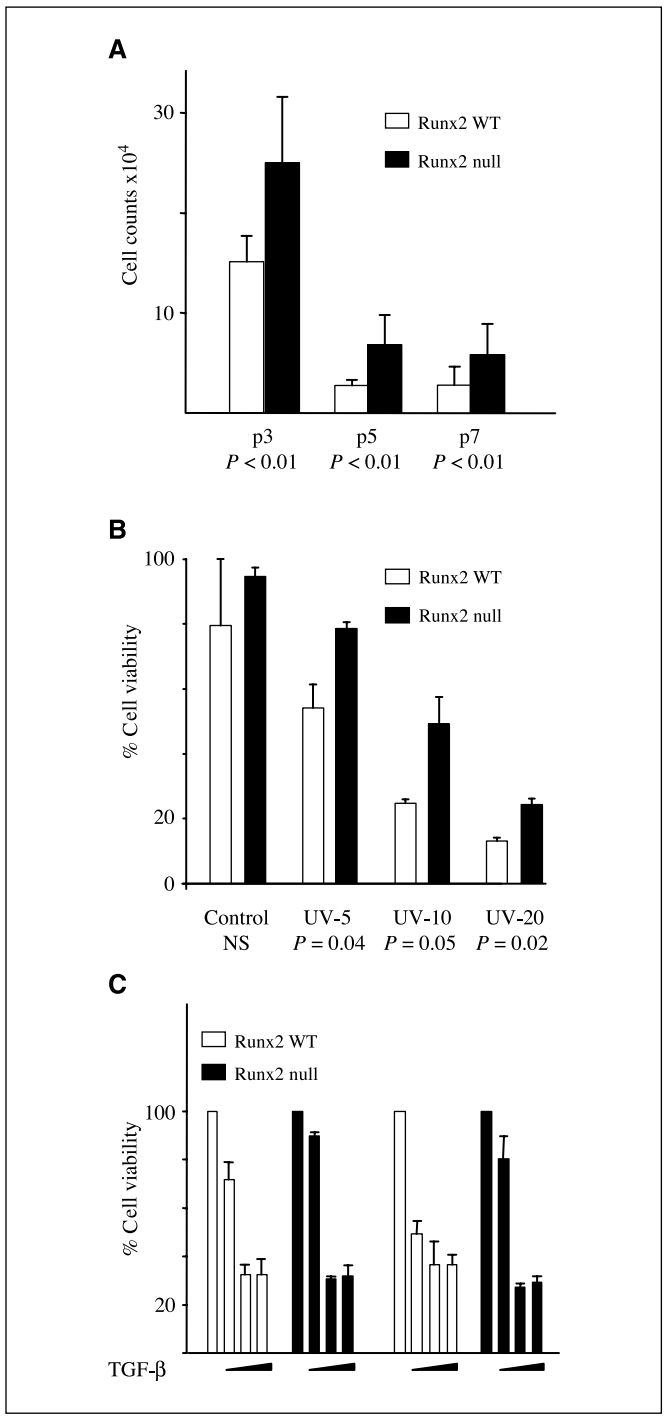

Figure 3. Loss of Runx2 conveys a growth advantage that is resistant to certain cellular stresses but not to TGF-β–mediated growth inhibition. *A,* total viable cell counts at day 7 from six wild-type and six *Runx2*$^{-/-}$ lines plated in triplicate at passages 3, 5, and 7. *B, Runx2*$^{-/-}$ fibroblasts are more resistant to UVC-induced cell death than wild-type controls. Two *Runx2*$^{-/-}$ and two wild-type cultures were plated in triplicate in 60-mm dishes and irradiated with 5, 10, and 20 J/m^2 UVC irradiation. Live/dead cell counts were performed by trypan blue exclusion after 24 h in culture. Similar results were obtained in two independent experiments. *C,* the growth of *Runx2*$^{-/-}$ and wild-type fibroblasts was inhibited by TGF-β. 5 ng/mL, 0.5 ng/mL, or 0.05 ng/mL TGF-β was added to triplicate wells on days 1, 3, 5, and 6, and total viable cell counts were calculated on day 7 by trypan blue exclusion. Control cultures were fed fresh medium in parallel. The histogram is a representative of two independent experiments. Replicate experiments on three independent *Runx2*$^{-/-}$ and wild-type lines performed with 5 ng/mL TGF-β gave essentially identical results.

impairment in TGF-β growth arrest over a range of concentrations (Fig. 3*C*).

Loss of *Runx2* permits escape from H-Ras^{V12}–induced senescence and oncogenic transformation. Because the *Runx* genes are potent agonists of premature senescence and *Runx2* disruption confers differential sensitivity to certain stress signaling pathways in primary MEFs, we investigated the effect of *Runx2* loss on the well-characterized phenomenon of Ras oncogene–induced senescence. As shown in Fig. 4*A*, expression of H-Ras^{V12} in the wild-type cell background induced growth stasis after an initial proliferative burst that was comparable with the vector-transduced controls. In contrast, *Runx2*$^{-/-}$ lines expressing H-Ras^{V12} displayed a 24-fold expansion in cell number over the same period and, unlike wild-type cells, were negative for SA-β-gal staining (Fig. 4*A*). The contrasting effects were not due to differential levels of H-Ras^{V12} expression as wild-type and *Runx2*$^{-/-}$ lines expressed comparable levels of H-Ras^{V12} by Western blotting. Also, *Runx2*$^{-/-}$ cells were not intrinsically resistant to growth stasis as reintroduction of Runx2 induced a senescent-like growth arrest and β-galactosidase staining in a manner indistinguishable from wild-type controls (Fig. 4*B*).

To determine whether Runx2 loss and H-Ras^{V12} can collaborate in the oncogenic transformation of MEFs, H-Ras^{V12} expressing *Runx2*$^{-/-}$ and wild-type cells were seeded in soft agar. As shown in Fig. 4*C*, anchorage-independent growth was significantly enhanced in H-Ras^{V12}/*Runx2*$^{-/-}$ cells compared with H-Ras^{V12}/ wild-type cells. The enhanced growth potential of H-Ras^{V12}/*Runx2*$^{-/-}$ cells was also seen in colony formation assays where these cells showed a much higher frequency of colony growth after low-density plating (data not shown). To determine whether loss of Runx2 renders primary MEFs susceptible to tumorigenesis *in vivo*, H-Ras^{V12}/*Runx2*$^{-/-}$, H-Ras^{V12}/wild-type, and vector control cells were transplanted into athymic mice. While no tumor growth occurred with cells carrying the empty vector (control cells, 0 of 6; *Runx2*$^{-/-}$ cells, 0 of 6) or wild-type cells expressing H-Ras^{V12} (0 of 6), those cells null for *Runx2* and expressing H-Ras^{V12} invariably produced tumors (6 of 6). Although most tumors appeared within 2 to 4 weeks, it was notable that these generally remained small and dormant before a later phase of expansion and vigorous growth. Examination of the rapidly growing tumors revealed a heterogeneous pattern with loss of expression of p16, p21, and/or p53 (data not shown). Although *Runx2* loss is clearly sufficient to allow Ras-induced tumors to arise, it seems that the transformed cells are not immortalized and that additional events are necessary for tumor progression.

Loss of Runx2 does not block induction of cell cycle inhibitors but nevertheless disables cell cycle checkpoint controls in response to H-Ras^{V12}. H-Ras^{V12}–induced premature senescence is accompanied by activation of p38 MAPK (27, 28) and the induction of p53, p19^{ARF}, p16^{INK4a}, and p21^{WAF1} (16). To determine whether these responses are intact in *Runx2*$^{-/-}$ MEFs, we examined the levels of activated p38 MAPK using an antibody that specifically recognizes phospho Thr^{180} and Tyr^{182} p38 MAPK, previously shown to represent the active kinase (29). As shown in Fig. 5*A*, phospho-p38 MAPK was readily detectable in wild-type MEFs. The levels exceeded that of our positive control but could not be further induced by H-Ras^{V12}, indicating high endogenous activation of this stress signaling cascade. Activation of p38 MAPK was similarly high in *Runx2*$^{-/-}$ fibroblasts but, in contrast to wild-type controls, could be further activated by H-Ras^{V12} (Fig. 5*A*). *In vitro* kinase assays using Activating Transcription Factor 2 as a

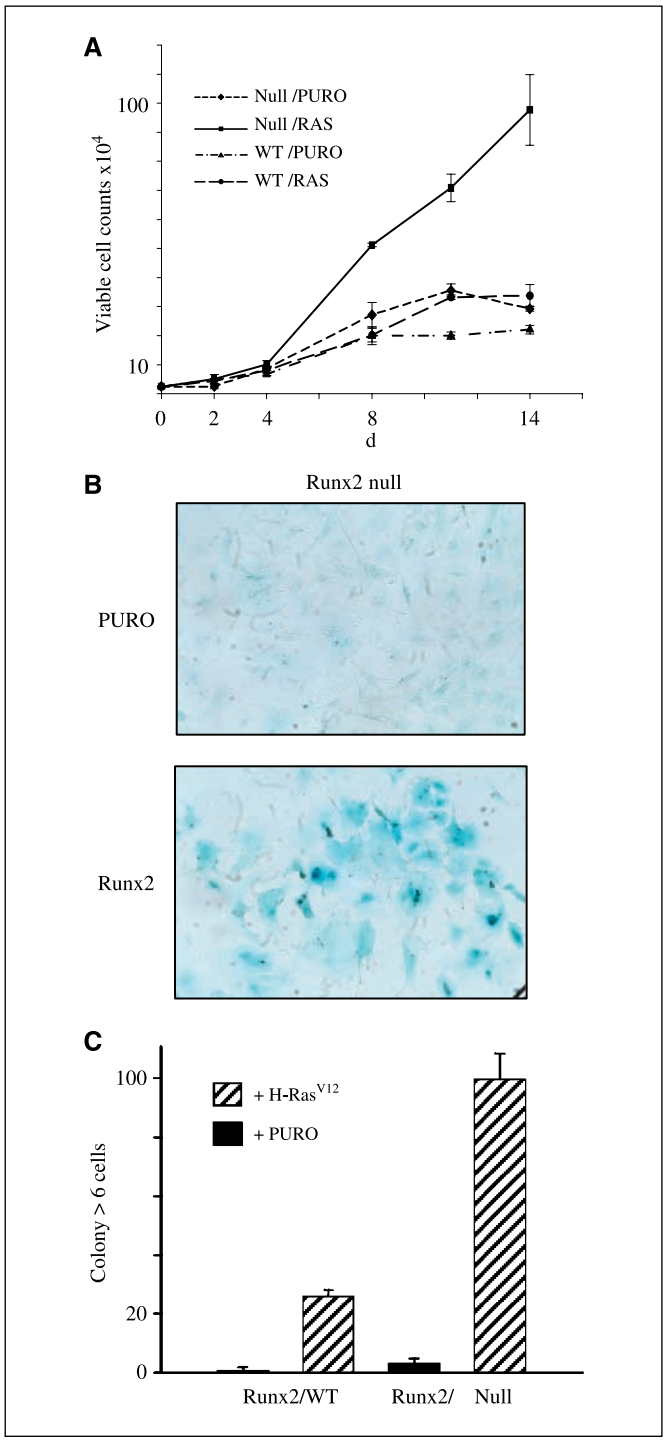

Figure 4. *Runx2*$^{-/-}$ cells expressing H-Ras^{V12} fail to undergo senescence. *A*, *Runx2*$^{-/-}$ and wild-type cells were transduced with a vector encoding *H-Ras^{V12}* or a control vector containing only the *PURO*-selectable gene. Passage 4 growth curves over 14 d, showing viable cell numbers. Similar results were obtained in four independent experiments using littermate-matched *Runx2*$^{-/-}$ and wild-type lines. *B*, SA-β-gal activity of *Runx2*$^{-/-}$ cells transduced with a vector encoding murine *Runx2*. Transduction with the control vector containing only the *PURO*-selectable gene failed to generate positively stained cultures. Photographs are at the same magnification. *C*, colony formation of *Runx2*$^{-/-}$ fibroblasts retrovirally transduced with H-Ras^{V12}. Cells were transduced with a retrovirus encoding *H-Ras^{V12}* or a control vector containing only the *PURO*-selectable gene and analyzed for oncogenic transformation. Numbers were determined for agar colonies (>0.1 mm) derived from plating 10^3 cells per 60-mm dish and fed every 3 to 4 d for 5 wk. *Error bars*, the average number of colonies derived from three independent dishes.

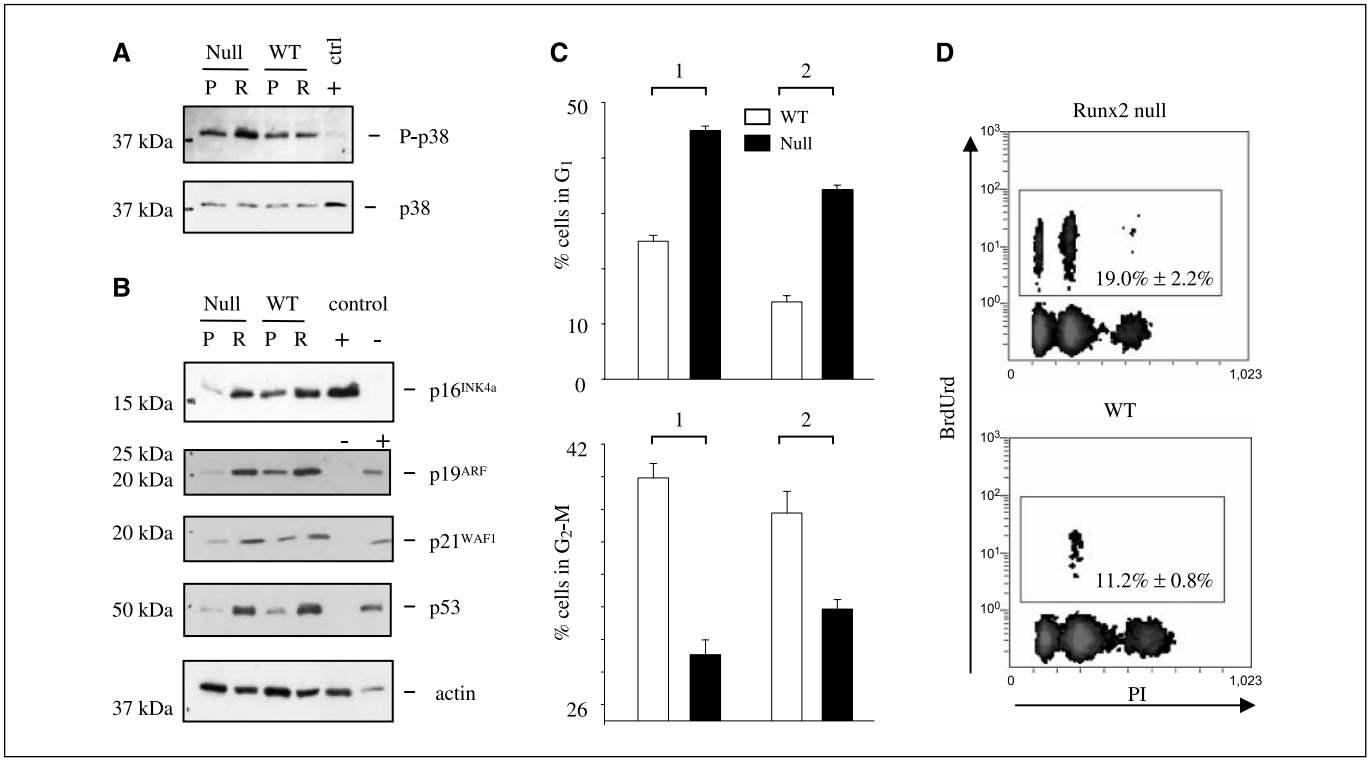

Figure 5. Loss of *Runx2* does not block the induction of growth arrest pathways by Ras but facilitates transit through S-G_2-M. *A,* total protein was extracted from early passage (p4) littermate-matched *Runx2*$^{-/-}$ and wild-type lines transduced with *H-Ras*^{V12} (*R*) or the *PURO* (*P*) vector control and probed against antibodies to phospho-p38 MAPK or p38 MAPK as a loading control. The Western blot is representative of two independent experiments. *B,* Western blot analysis as in *A* probed against antibodies to p16^{INK4a}, p19^{ARF}, p21^{WAF1}, and p53. Actin was used as a loading control. *C,* cell cycle analysis of H-Ras^{V12}–transduced wild-type and *Runx2*$^{-/-}$ MEFs is shown as the percentage of propidium iodide stained cells with 2N (*top*) and 4N (*bottom*) DNA content at day 13 after transduction. Two independent littermate-matched wild-type and *Runx2*$^{-/-}$ cultures are grouped (*1* and *2*). *Error bars,* triplicate samples. Similar results from two independent experiments. *D,* cytometry density plots of *Runx2*$^{-/-}$ (*top*) and wild-type (*bottom*) cells transduced with H-Ras^{V12} that were labeled with BrdUrd for 15 h. Percentage of BrdUrd incorporation is given based on triplicate samples. Identical results were seen with two independent wild-type and *Runx2*$^{-/-}$ samples.

substrate confirmed it to be fully functional (data not shown), indicating that signaling between H-Ras^{V12} and p38 MAPK remained intact in *Runx2*$^{-/-}$ MEFs. An examination of the expression levels of p53, p19^{ARF}, p16^{INK4a}, and p21^{WAF1} revealed that despite lower basal levels in the *Runx2*$^{-/-}$ genetic background, H-Ras^{V12} induced p53, p19^{ARF}, p16^{INK4a}, and p21^{WAF1} to a comparable level in both *Runx2*$^{-/-}$ and wild-type control cells (Fig. 5*B*). Therefore, although Runx2 is essential for H-Ras^{V12} to exert its growth suppressing function, it does not seem to be required for the induction of a panel of genes that have been shown to contribute to the growth arrest.

In contrast, cell cycle analysis confirmed and elucidated a profound difference in the growth response of the *Runx2*$^{-/-}$ cells to H-Ras^{V12}. Propidium iodide staining revealed a higher proportion of cells with a 2N (G_1) DNA content and a significantly lower proportion of cells with a 4N (G_2-M) DNA content in *Runx2*$^{-/-}$ cells compared with controls (Fig. 5*C*). Dual staining with propidium iodide and BrdUrd showed higher rates of BrdUrd incorporation in *Runx2*$^{-/-}$ H-Ras^{V12} cultures, consistent with their observed expansion in cell numbers during the culture period (Fig. 5*D*). Of these cells, a significant proportion displayed a 2N DNA content, indicating successful transit through G_2-M. A striking difference was seen in the wild-type cultures that displayed a much lower number of BrdUrd positive cells with a 2N DNA content. Together these results show that the H-Ras^{V12} expressing *Runx2*$^{-/-}$ cells are actively cycling, while a significant proportion of wild-type cells are delayed or arrested during transit through S-G_2-M.

Loss of Runx2 confers increased expression of S-G_2-M cyclins and associated cyclin-dependent kinase activities. The continued cycling of *Runx2*$^{-/-}$ cells in the presence of a cascade of growth inhibitors suggested a compensatory mechanism possibly involving constitutive expression of positive growth mediators. We therefore compared the levels of cyclin gene expression in the wild-type and *Runx2*$^{-/-}$ genetic backgrounds. Quantitative reverse transcription-PCR (qRT-PCR) analysis showed that cyclin D1 expression was unaffected by Runx2 status, although it was up-regulated by H-Ras^{V12} as previously reported (Fig. 6*A*). However, the expression levels of cyclins A2 (Fig. 6*B*), B1 (Fig. 6*C*), and E1 (Fig. 6*D*) mRNA were all markedly up-regulated in *Runx2*$^{-/-}$ fibroblasts compared with wild-type controls (Fig. 6*A*). Moreover, unlike wild-type cells where expression of these cyclins declined steadily throughout the culture period, high levels of cyclin E1, cyclin A2, and cyclin B1 mRNA were sustained in *Runx2*$^{-/-}$ MEFs and persisted even as the cells reached confluence. Strikingly, deregulation of cyclin levels was observed in *Runx2*$^{-/-}$ cells whether or not they expressed H-Ras^{V12}.

To determine whether cyclin-dependent kinase activity was also deregulated in the absence of Runx2, *in vitro* kinase assays were performed using histone H1 as a substrate. As shown in the parallel panels, elevated levels of A-, B1-, and E-dependent kinase activities were observed in *Runx2*$^{-/-}$ cells

relative to wild-type controls after coimmunoprecipitation with the corresponding antibody. Comparable results were also obtained upon retroviral transduction with H-Ras^{V12}. A direct analysis of the kinase complex composition was problematic due to comigration of cyclin proteins with the IgG heavy chain moiety, but examination of cyclin protein expression by Western blotting confirmed the qRT-PCR data, thereby supporting a direct relationship between cyclin gene expression

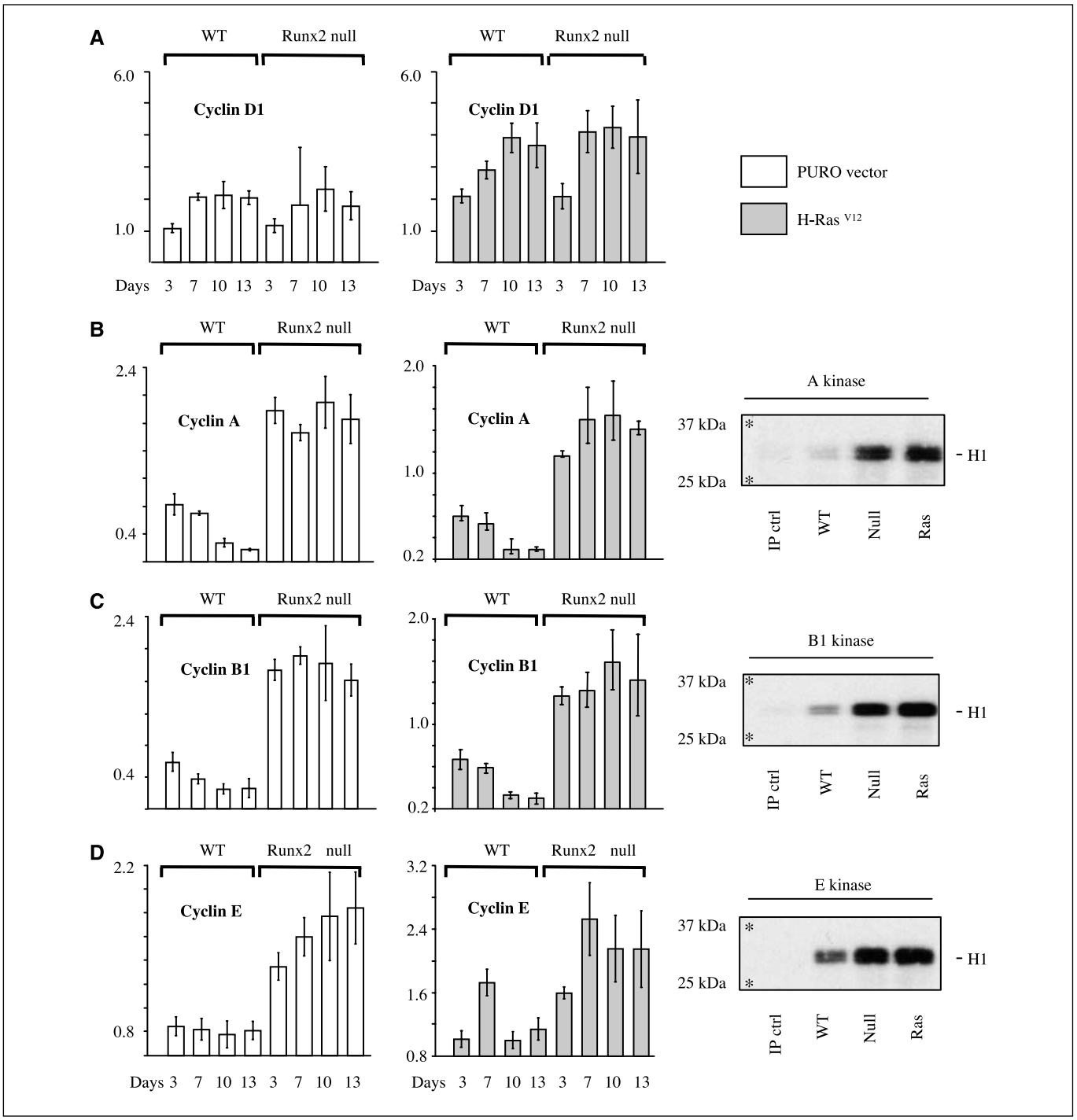

Figure 6. Loss of Runx2 confers increased expression of S-G_2-M cyclins and associated cyclin-dependent kinase activities. *A,* cyclin D1 expression is refractory to loss of Runx2 but remains sensitive to induction by H-Ras^{V12}. cDNA was prepared from littermate-matched *Runx2*$^{-/-}$ and wild-type cultures transduced with *H-Ras*^{V12} or the *PURO* control vector and plated for 0 to 13 d in culture. Cyclin D1 expression was assayed at each time point by relative quantification to endogenous control hprt and calibrated to the day 0 wild-type sample. *B* to *D,* loss of Runx2 confers increased expression of cyclin A2 (*B*), cyclin B1 (*C*), and cyclin E1 (*D*) and sustains downstream cyclin dependent kinase activity. cDNA was analyzed from the same data set as described in *A*. The data are displayed as raw RQ values and is representative of two independent experiments on two littermate-matched *Runx2*$^{-/-}$ and wild-type lines. Parallel cultures were harvested for immunoprecipitation kinase assays of total cyclin A–, cyclin B1–, and cyclin E–associated kinase activities. Cell extracts were immunoprecipitated with antibodies specific for the relevant cyclin, and the precipitates were analyzed for kinase activity using histone H1 (32 kDa) as a substrate. *, 25 and 37 kDa molecular weight markers. Data are representative of two independent experiments.

levels and S-G_2-M cyclin-dependent kinase activities in *Runx2*$^{-/-}$ cells. cells.

Discussion

In this study, we have shown that Runx2 can induce premature senescence in primary MEFs, revealing a further functional attribute shared by the *Runx* gene family. This process is markedly different from Ras-induced senescence that occurs in response to aberrant proliferation and DNA damage signaling (ref. 22 and references therein), and it seems that Runx signaling induces a senescence cascade downstream of these responses. However, the process remains dependent on p53, and our finding that p53 is required for Runx2-induced senescence recapitulates previous results for RUNX1 (11). More surprising is our finding that Runx2 has a nonredundant role in MEFs where gene disruption promotes immortalization, disables Ras-induced senescence, and facilitates oncogenic transformation. These findings offer a new perspective on the lineage-specific tumor suppressor activities of the *Runx* gene family.

Runx2$^{-/-}$ MEFs display enhanced proliferation, but it is important to note that this phenomenon was observed on a background of primary cultures that display low proliferative rates compared with established cell lines. The early growth advantage was refractory to the nonphysiologic conditions of *in vitro* culture (23, 24) but was amplified by low-dose UVC irradiation, suggesting that loss of *Runx2* alters sensitivity to a subset of stress-signaling pathways. The early growth advantage of *Runx2*$^{-/-}$ cells may be sufficient to account for their increased susceptibility to become immortalized at much higher rates than wild-type cultures, although a more direct role in regulating cellular life span or replicative senescence in response to telomere shortening cannot be formally excluded. However, it is clear that immortalized *Runx2*$^{-/-}$ cells remain nontumorigenic, unlike their *p53*$^{-/-}$ counterparts, suggesting that this tumor suppressor–like property of *Runx2* is likely to be less potently manifested *in vivo*. Another interesting contrast is that *Runx2*$^{-/-}$ cells retain full sensitivity to the growth inhibitory effects of TGF-β, whereas *p53*$^{-/-}$ cells are refractory (30). Whether Runx function is dispensable for TGF-β inhibition in primary MEFs or this process is mediated by low-level expression of another family member remains to be determined.

Escape from senescence in response to exogenous H-Ras^{V12} is the most striking attribute of *Runx2*$^{-/-}$ cells. We have established that this phenotype is not due to an intrinsic loss of capacity to undergo senescence as *Runx2*$^{-/-}$ lines remain susceptible to senescence induced by ectopic expression of Runx2. However, attempts to identify the basis of their resistance to H-Ras^{V12} revealed some unanticipated results. In wild-type MEFs, H-Ras^{V12}–induced senescence is accompanied by activation of the p38 MAPK signaling cascade (28) and the induction of p16^{INK4a}, p19^{ARF}, p21^{WAF1}, and p53 (16). We found no obvious defect in these responses in *Runx2*$^{-/-}$ MEFs that express high levels of the active p38 MAPK and accumulate all four proteins to similar levels in response to H-Ras^{V12}. In fact, there was evidence of hyperactivation of p38 MAPK in *Runx2*$^{-/-}$ cells, suggestive of the loss of a feedback control mechanism. These findings were somewhat surprising as at least two of the genes involved have been implicated as direct targets for Runx regulation (12, 31, 32), and *Runx2*$^{-/-}$ MEFs expressed slightly lower basal levels of all of these markers. It seems that Runx2 is dispensable for the induction of this cascade of inhibitory signals by H-Ras^{V12}, and that the explanation for the continued proliferation of *Runx2*$^{-/-}$ cells must lie elsewhere downstream.

Analysis of other components of the cell cycle machinery provided us with a clear rationale for the aberrant growth properties of *Runx2*$^{-/-}$ cultures, as these cells were found to express high levels of cyclin A2, B1, and E1 that were refractory to down-regulation by Ras. Moreover, the corresponding cyclin-associated cyclin-dependent kinase activities were markedly elevated on the *Runx2*$^{-/-}$ background. Although earlier studies of H-Ras^{V12}–induced senescence have described a G_1 arrest as the predominant feature (16, 33), cell cycle analysis of our MEF cultures revealed stronger evidence of a block at G_2-M in wild-type cells, with accumulation of cells with a 4N DNA content, whereas *Runx2*$^{-/-}$ cells continued to cycle. Our observations do not exclude the existence of multiple blocks to cell cycle progression in H-Ras^{V12}–transduced cells but are in accord with recent studies showing that oncogene-induced senescence and associated DNA damage can result in activation of S-G_2-M checkpoints (34, 35).

A precedent for the ability of deregulated cyclin expression to overcome the Ras-induced inhibitory cascade has been provided by two genes discovered in screens for mediators of escape from Ras-induced senescence. Thus, hDRIL binds E2F1 and activates the cyclin E1 promoter (36), whereas repression of BTG2 leads to up-regulation of cyclins D1 and E1 (37). Similarly, it now seems that the constitutive expression and/or lack of silencing of several cyclin genes underlie the resistance of *Runx2*$^{-/-}$ cells to culture stress and Ras-induced growth arrest. It is interesting to note that cyclin A2 is among the E2F-regulated genes that are sequestered in senescence-associated heterochromatic foci (38, 39), which appear in the course of a multistep process, leading to irreversible loss of replicative capacity in human fibroblasts. The possibility that Runx functions are required in this critical program merits further investigation, particularly in light of evidence implicating Runx2 in SWI/SNF chromatin remodeling in osteoblast differentiation (40). It is conceivable that other defects in Runx2 null cells also contribute to their resistance to Ras-induced senescence. A recent study in human fibroblasts has shown that Ras-induced senescence requires attenuation of MAPK and PI3K signaling in addition to induction of cell cycle inhibitors (41), and it is intriguing to note that we observed elevated p38 MAPK signaling in Runx2 null cells in the presence of Ras.

This study also has wider implications for the role of the *Runx* genes in cancer. Because all three genes induce premature senescence when expressed ectopically, the prospect of a similar redundant role for the endogenous *Runx* genes in the induction of the senescence program in response to oncogene-induced growth arrest merits further investigation. It may be expected that manifestations of loss of Runx expression or function will be limited to those tissues where a single family member plays a decisive role, as we have found for *Runx2* in MEFs. Whether Runx2 loss or silencing is associated with specific cancers *in vivo* is an interesting question. As this gene plays a critical role *in vivo* in the development of chondrogenic and osteogenic tissues, its tumor protective action might be manifested in mesenchymal tissues. With regard to other family members, it is notable that *RUNX1* loss of function mutations have been associated with activated Ras signaling in AML and myelodysplastic syndrome/AML (42, 43). In addition, epithelial cancers that have been

associated with RUNX3 down-regulation (ref. 2 and references therein) display Ras pathway mutations at significant frequencies, suggesting the possibility of parallel roles for the other Runx family members. It will also be interesting to explore the Runx2-dependent growth arrest mechanism uncovered here for its relevance to the normal physiologic roles of the *Runx* genes in cell fate determination, particularly where these entail checks to the proliferation of stem cells or early progenitors to permit lineage-specific differentiation (44).

Acknowledgments

Received 8/7/2007; revised 9/19/2007; accepted 9/26/2007.

Grant support: Major support for this work was provided by a joint programme grant from Cancer Research UK and the Leukaemia Research Fund, while some aspects were supported by a project grant from the Association for International Cancer Research.

The costs of publication of this article were defrayed in part by the payment of page charges. This article must therefore be hereby marked *advertisement* in accordance with 18 U.S.C. Section 1734 solely to indicate this fact.

We thank Dr. Ming Hu for preliminary observations, Sharon Mackay and Nancy Mackay for their excellent technical assistance, and Professor David Gillespie for reagents and helpful discussions.

References

1. Gergen JP, Butler BA. Isolation of the *Drosophila* segmentation gene runt and analysis of its expression during embryogenesis. Genes Dev 1988;2:1179–93.
2. Blyth K, Cameron ER, Neil JC. The Runx gene family: gain or loss of function in cancer. Nat Rev Cancer 2005; 5:376–87.
3. Stewart M, Terry A, Hu M, et al. Proviral insertions induce the expression of bone-specific isoforms of PEBP2αA (CBFA1): evidence for a new myc collaborating oncogene. Proc Natl Acad Sci U S A 1997;94:8646–51.
4. Stewart M, Mackay N, Cameron ER, Neil JC. The common retroviral insertion locus Dsi1 maps 30 kb upstream of the P1 promoter of the murine Runx3/Cbfa3/Aml2 gene. J Virol 2002;76:4364–9.
5. Wotton S, Stewart M, Blyth K, et al. Proviral insertion indicates a dominant oncogenic role for Runx1/AML1 in T-cell lymphoma. Cancer Res 2002;62:7181–5.
6. Blyth K, Vaillant F, Mackay N, et al. Runx2 and MYC collaborate in lymphoma development by suppressing apoptotic and growth arrest pathways *in vivo*. Cancer Res 2006;66:2195–201.
7. Growney JD, Shigematsu H, Li Z, et al. Loss of Runx1 perturbs adult hematopoiesis and is associated with a myeloproliferative phenotype. Blood 2005;106:494–504.
8. Miyazono K, Maeda S, Imamura T. Coordinate regulation of cell growth and differentiation by TGF-β superfamily and Runx proteins. Oncogene 2004;23:4232–7.
9. Ito Y, Miyazono K. RUNX transcription factors as key targets of TGF-β superfamily signaling. Curr Opin Genet Dev 2003;13:43–7.
10. Blyth K, Terry A, Mackay N, et al. Runx2: a novel oncogenic effector revealed by *in vivo* complementation and retroviral tagging. Oncogene 2001;20:295–302.
11. Wotton S, Blyth K, Kilbey A, et al. RUNX1 transformation of primary embryonic fibroblasts is revealed in the absence of p53. Oncogene 2004;23:5476–86.
12. Linggi B, Muller-Tidow C, van de LL, et al. The t(8;21) fusion protein, AML1 ETO, specifically represses the transcription of the p14(ARF) tumor suppressor in acute myeloid leukemia. Nat Med 2002;8:743–50.
13. Hemann MT, Narita M. Oncogenes and senescence: breaking down in the fast lane. Genes Dev 2007;21:1–5.
14. Michaloglou C, Vredeveld LCW, Soengas MS, et al. BRAF(E600)-associated senescence-like cell cycle arrest of human naevi. Nature 2005;436:720–4.
15. Chen ZB, Trotman LC, Shaffer D, et al. Crucial role of p53-dependent cellular senescence in suppression of Pten-deficient tumorigenesis. Nature 2005;436:725–30.
16. Serrano M, Lin AW, McCurrach ME, Beach D, Lowe SW. Oncogenic ras provokes premature cell senescence associated with accumulation of p53 and p16(INK4a). Cell 1997;88:593–602.
17. Otto F, Thornell AP, Crompton T, et al. Cbfa1, a candidate gene for cleidocranial dysplasia syndrome, is essential for osteoblast differentiation and bone development. Cell 1997;89:765–71.
18. Morgenstern JP, Land H. Advanced mammalian gene transfer: high titre retroviral vectors and a complementary helper-free packaging cell line. Nucleic Acids Res 1990;18:3587–96.
19. Todaro GJ, Green H. Quantitative studies of growth of mouse embryo cells in culture and their development into established lines. J Cell Biol 1963;17:299–313.
20. Blyth K, Stewart M, Bell M, et al. Sensitivity to Myc-induced apoptosis is retained in spontaneous and transplanted lymphomas of CD2-mycER mice. Oncogene 2000;19:773–82.
21. Clark W, Black EJ, MacLaren A, et al. v-Jun overrides the mitogen dependence of S-phase entry by deregulating retinoblastoma protein phosphorylation and E2F-pocket protein interactions as a consequence of enhanced cyclin E-cdk2 catalytic activity. Mol Cell Biol 2000;20:2529–42.
22. Yaswen P, Campisi J. Oncogene-induced senescence pathways weave an intricate tapestry. Cell 2007;128: 233–4.
23. Sherr CJ, DePinho RA. Cellular senescence: mitotic clock or culture shock? Cell 2000;102:407–10.
24. Ramirez RD, Morales CP, Herbert BS, et al. Putative telomere-independent mechanisms of replicative aging reflect inadequate growth conditions. Genes Dev 2001; 15:398–403.
25. Torquati A, O'Rear L, Longobardi L, Spagnoli A, Richards WO, Beauchamp RD. RUNX3 inhibits cell proliferation and induces apoptosis by reinstating transforming growth factor β responsiveness in esophageal adenocarcinoma cells. Surgery 2004;136:310–6.
26. Chi XZ, Yang JO, Lee KY, et al. RUNX3 suppresses gastric epithelial cell growth by inducing p21(WAF1/Cip1) expression in cooperation with transforming growth factor β-activated SMAD. Mol Cell Biol 2005; 25:8097–107.
27. Wang WP, Chen JX, Liao R, et al. Sequential activation of the MEK-extracellular signal-regulated kinase and MKK3/6-p38 mitogen-activated protein kinase pathways mediates oncogenic ras-induced premature senescence. Mol Cell Biol 2002;22:3389–403.
28. Bulavin DV, Kovalsky O, Hollander MC, Fornace AJ. Loss of oncogenic H-ras-induced cell cycle arrest and p38 mitogen-activated protein kinase activation by disruption of gadd45a. Mol Cell Biol 2003;23:3859–71.
29. Raingeaud J, Gupta S, Rogers JS, et al. Pro-inflammatory cytokines and environmental-stress cause P38 mitogen-activated protein-kinase activation by dual phosphorylation on tyrosine and threonine. J Biol Chem 1995;270:7420–6.
30. Cordenonsi M, Dupont S, Maretto S, Insinga A, Imbriano C, Piccolo S. Links between tumor suppressors: p53 is required for TGF-β gene responses by cooperating with Smads. Cell 2003;113:301–14.
31. Lutterbach B, Westendorf JJ, Linggi B, Isaac S, Seto E, Hiebert SW. A mechanism of repression by acute myeloid leukemia-1, the target of multiple chromosomal translocations in acute leukemia. J Biol Chem 2000;275: 651–6.
32. Westendorf JJ, Zaidi SK, Cascino JE, et al. Runx2 (Cbfa1, AML-3) interacts with histone deacetylase 6 and represses the p21(CIP1/WAF1) promoter. Mol Cell Biol 2002;22:7982–92.
33. Mason DX, Jackson TJ, Lin AW. Molecular signature of oncogenic ras-induced senescence. Oncogene 2004; 23:9238–46.
34. Di Micco R, Fumagalli M, Cicalese A, et al. Oncogene-induced senescence is a DNA damage response triggered by DNA hyper-replication. Nature 2006;444: 638–42.
35. Bartkova J, Rezaei N, Liontos M, et al. Oncogene-induced senescence is part of the tumorigenesis barrier imposed by DNA damage checkpoints. Nature 2006;444: 633–7.
36. Peeper DS, Shvarts A, Brummelkamp T, et al. A functional screen identifies hDRIL1 as an oncogene that rescues RAS-induced senescence. Nat Cell Biol 2002;4: 148–53.
37. Boiko AD, Porteous S, Razorenova OV, Krivokrysenko VI, Williams BR, Gudkov AV. A systematic search for downstream mediators of tumor suppressor function of p53 reveals a major role of BTG2 in suppression of Ras-induced transformation. Genes Dev 2006;20: 236–52.
38. Narita M, Nunez S, Heard E, et al. Rb-mediated heterochromatin formation and silencing of E2F target genes during cellular senescence. Cell 2003;113:703–16.
39. Zhang RG, Chen W, Adams PD. Molecular dissection of formation of senescence-associated heterochromatin foci. Mol Cell Biol 2007;27:2343–58.
40. Young DW, Pratap J, Javed A, et al. SWI/SNF chromatin remodeling complex is obligatory for BMP2-induced, Runx2-dependent skeletal gene expression that controls osteoblast differentiation. J Cell Biochem 2005;94:720–30.
41. Courtois-Cox S, Williams SMG, Reczek EE, et al. A negative feedback signaling network underlies oncogene-induced senescence. Cancer Cell 2006;10:459–72.
42. Roumier C, Lejeune-Dumoulin S, Renneville A, et al. Cooperation of activating RAS/rtk signal transduction pathway mutations and inactivating myeloid differentiation gene mutations in M0 AML: a study of 45 patients. Leukemia 2006;20:433–6.
43. Niimi H, Harada H, Harada Y, et al. Hyperactivation of the RAS signaling pathway in myelodysplastic syndrome with AML1/RUNX1 point mutations. Leukemia 2006;20:635–44.
44. Pratap J, Galindo M, Zaidi SK, et al. Cell growth regulatory role of Runx2 during proliferative expansion of preosteoblasts. Cancer Res 2003;63:5357–62.